Chemistry Central Journal

RESEARCH ARTICLE   **Open Access**

Structural characterization of vanadium oxide catalysts supported on nanostructured silica SBA-15 using X-ray absorption spectroscopy

Anke Walter[1], Rita Herbert[2], Christian Hess[2,3], Thorsten Ressler[1*]

Abstract

The local structure of vanadium oxide supported on nanostructured SiO_2 (V_xO_y/SBA-15) was investigated by in situ X-ray absorption spectroscopy (XAS). Because the number of potential parameters in XAS data analysis often exceeds the number of "independent" parameters, evaluating the reliability and significance of a particular fitting procedure is mandatory. The number of independent parameters (Nyquist) may not be sufficient. Hence, in addition to the number of independent parameters, a novel approach to evaluate the significance of structural fitting parameters in XAS data analysis is introduced. Three samples with different V loadings (i.e. 2.7 wt %, 5.4 wt %, and 10.8 wt %) were employed. Thermal treatment in air at 623 K resulted in characteristic structural changes of the V oxide species. Independent of the V loading, the local structure around V centers in dehydrated V_xO_y/SBA-15 corresponded to an ordered arrangement of adjacent V_2O_7 units. Moreover, the V_2O_7 units were found to persist under selective oxidation reaction conditions.

Background

Mixed transitions metal oxides (e.g. MoVNbTe oxides) are active in selective oxidation of propane to acrylic acid. In contrast to various binary oxides (e.g. MoO_3 or V_2O_5), these mixed oxides exhibit a much higher selectivity. However, the origin of the promoting effect of, for instance, vanadium in mixed oxides is largely unknown. Hence, model systems are sought which enable conclusions on structure activity relationships of individual metal centers in active catalysts. For that, supported metal oxides possess two major advantages over bulk oxides. First, particular metal oxide structures which are not readily available for investigations under reaction conditions can be stabilized and studied on suitable support materials [1]. Second, dispersed supported metal oxides simplify correlating the local structure around the metal centers with their catalytic performance. Distinguishing active metal centers at the surface from metal centers in the bulk of conventional oxide catalysts is no longer required.

V_xO_y supported on SBA-15 (nanostructured SiO_2) [2] constitutes a suitable model system to investigate the role of vanadium during selective oxidation catalysis [3-6]. Structural characterization of V_xO_y supported on SiO_2 has been subject of many spectroscopic studies including IR [[7-9], XPS [6,10,11], Raman [10-15], UV-VIS [11,13-16] and EXAFS [13,17-22]. A recent review of spectroscopic investigations and structural characteristics of various supported vanadium oxides has been presented by Weckhuysen and Keller [23]. It is assumed, that the structure of supported vanadium oxide depends on both amount of vanadium and degree of hydration [14]. Hence, most studies were performed on V_xO_y/SiO_2 samples exhibiting low vanadium loading (< 10 wt %). At these loadings a monolayer of supported V_xO_y species is assumed and crystalline V_2O_5 is not detectable. Under ambient conditions the structure of hydrated vanadium oxide supported on SiO_2 resembles that of V_2O_5 [10,13,18]. Thermal treatment in oxygen results in dehydration of the vanadium oxide species. This dehydrated state has been proposed to consist of isolated VO_4 tetrahedrons bond to the SiO_2 support [13,17,24,25]. However, V_2O_7 dimers or further extended structures supported on SiO_2 have not been excluded [15]. In total, the structure of dehydrated vanadium oxide species supported on SiO_2 remains under debate.

* Correspondence: thorsten.ressler@tu-berlin.de
[1]Institut für Chemie, Technische Universität Berlin, Strasse des 17. Juni 135, 10623 Berlin, Germany

XAS is particularly suitable to study supported catalysts under reaction conditions. The average valence, for instance, can be readily obtained by comparison with known reference compounds. Elucidating the geometric structure, however, is often more difficult. In the conventional approach theoretical XAFS scattering amplitudes and phases are calculated for a suitable model structure. Subsequently, a sum of theoretical XAFS functions is refined to the experimental data. Structural parameters like coordination numbers, nearest neighbor distances, and disorder parameters may be determined. However, more often than not, the number of potential parameters exceeds the number of "independent" parameters. The upper limit may be calculated from Fourier theory and must not be exceeded. Nonetheless, it appears that even refinements employing a much smaller number of freely varied parameters may yield ambiguous structural results. The often used Nyquist criteria may not be sufficient to deem a fitting procedure reliable. Basically, one pair of strongly correlated parameters suffices to render a seemingly good agreement between experimental data and theoretical model structure meaningless. While this case may be clearly indicated by the correlation matrix of the refinement, other pitfalls may be less obvious. Hence, procedure are sought that enable evaluating the significance of each fitting parameter individually.

Here, we have performed in situ XAS investigations of V_xO_y supported on SBA-15 in the hydrated and dehydrated state. The same materials were already carefully characterized by several standard techniques (i.e. physisorption, TEM, IR, Raman, UV-Vis, and XPS) and the results of these studies have been described in Ref [9,10,14]. In particular, using UV-Vis and Raman spectroscopy, Hess et al. showed that the catalysts are similar to other systems previously described in the literature. However, the results obtained could not unequivocally determine the local structure around the V species on SiO$_2$, as it was also the case in previous studies. Our approach focused on elucidating the local structure around the vanadium centers in the dehydrated state of V_xO_y-SBA-15 model catalysts with different vanadium loadings. A detailed XAFS data analysis, in particular of higher V-V distances, was performed together with a detailed evaluation of the significance of the fitting parameters employed. This procedure permitted detailed conclusions on the extended local structure of the vanadium oxide species supported on SBA-15.

Results and discussion
Local structure of dehydrated V_xO_y/SBA-15 - Comparison to V oxide references
Characterization of pore structure and surface area, and optical spectroscopic investigations of the same model

catalysts studied here have been previously described [9,10,14]. After surface functionalisation and ion exchange to introduce the V precursor, the materials were calcined at 823 K in air. Calcination results in decomposition of both precursor and functionalisation agent. Preparation, functionalisation, and thermal treatment also have been described in Ref [9,10,14]. The authors stated that residuals of the functionalisation agent were no longer detectable (i.e. IR, Raman, UV-Vis, and XPS) in the material obtained. A brief summary of the N$_2$ physisorption analysis described in Ref [10] is given in Table 1.

Here, we have performed a detailed XAFS investigation of samples with different V loadings in the hydrated and dehydrated state. In particular, we wanted to analyze the contribution of higher scattering shells to the XAFS signal and possibly reveal the presence of V nearest neighbors in the local structure of vanadium oxide species supported on SiO$_2$. A detailed XAFS analysis of higher shells in the FT(χ(k)*k^3) has been largely neglected in the corresponding literature.

During thermal treatment of as-prepared hydrated V_xO_y/SBA-15 in oxygen (20% in He) a loss of water and a distinct change in structure were observed. After thermal treatment dehydrated V_xO_y/SBA-15 was cooled to 293 K in oxygen in He without exposure to air or water. No changes in XAFS spectra were observed during cooling. The EXAFS χ(k)*k^3 of dehydrated V_xO_y/SBA-15 with different V loadings are depicted in Figure 1. The usable spectral ranged extended from 2.7 Å through 11.0 Å. The V K edge XANES spectra and the FT(χ(k)*k^3) of dehydrated V_xO_y/SBA-15 samples measured at 293 K are shown in Figure 2. FT(χ(k)*k^3) are not phase shift corrected. Thus, the distances in the FT(χ(k)*k^3) are shifted by ~0.4 Å to lower values compared to crystallographic distances. Compared to vanadium oxide references, the overall XANES region of dehydrated V_xO_y/SBA-15 resembled best those of NH$_4$VO$_3$, Mg$_2$V$_2$O$_7$, and Na$_3$VO$_4$ (Figure 3(a)). In the local structure of these references vanadium centers are tetrahedrally coordinated by four oxygen atoms. Compared to the XANES spectrum of dehydrated V_xO_y/SBA-15, NH$_4$VO$_3$ and Mg$_2$V$_2$O$_7$ exhibit very similar pre-edge peak heights in their XANES spectra (i.e. 0.65). Conversely, the pre-edge peaks in the XANES of Na$_3$VO$_4$ and Mg$_3$V$_2$O$_8$ are much higher than that of dehydrated V_xO_y/SBA-15 (Figure 3(a)).

In Figure 3(b) the FT(χ(k)*k^3) of NH$_4$VO$_3$, Mg$_2$V$_2$O$_7$, and Na$_3$VO$_4$ are compared to that of dehydrated V_xO_y/SBA-15. The first V-O peak in the FT(χ(k)*k^3) at ~1.4 Å (not phase shift corrected) for all references shown corresponds to a VO$_4$ tetrahedron in the respective structures. Apparently, the spectra of NH$_4$VO$_3$ and Mg$_2$V$_2$O$_7$ most closely resemble that of dehydrated

Table 1 N$_2$ physisorption analysis of supported vanadium oxide samples.

	Vanadium loading on SBA-15			S$_{BET}$ (m^2/g)	d$_P$ (nm)	V$_P$ (mL/g)
	(wt %)	V atoms/nm^2	(mmol/g)			
SBA-15	-	-	-	897	7.0	1.1
2.7 wt % V/SBA-15	2.7	0.7	0.53	445	6.7	0.5
5.4 wt % V/SBA-15	5.4	1.4	1.05	440	6.6	0.5
10.8 wt % V/SBA-15	10.8	4.7	2.12	273	5.5	0.3

Vanadium loading, surface area (S$_{BET}$), pore diameter (d$_P$), and pore volume (V$_P$) of SBA-15 and vanadium oxides supported on SBA-15. Details have been presented in Ref [10].

V$_x$O$_y$/SBA-15. In the FT(χ(k)*k^3) of Na$_3$VO$_4$ and Mg$_3$V$_2$O$_8$ the first V-O peak is significantly higher than in the FT(χ(k)*k^3) of dehydrated V$_x$O$_y$/SBA-15. In contrast to the FT(χ (k)*k^3) of Mg$_3$V$_2$O$_8$ which exhibits a significant amplitude at distances above 2 Å, the FT(χ (k)*k^3) of Na$_3$VO$_4$, NH$_4$VO$_3$, Mg$_2$V$_2$O$_7$, and dehydrated V$_x$O$_y$/SBA-15 show little amplitude at higher distances. Moreover, looking at the differences between the FT(χ (k)*k^3) of Na$_3$VO$_4$, NH$_4$VO$_3$, and Mg$_2$V$_2$O$_7$, the latter appears to yield the best agreement with that of dehydrated V$_x$O$_y$/SBA-15. In all reference the low amplitude of the FT(χ (k)*k^3) at R > 2 Å is characteristic of the local structure around the V centers. It is not caused by an increased amount of disorder. In total, based on comparing the XANES and FT(χ (k)*k^3) of dehydrated V$_x$O$_y$/SBA-15 to those of potential references, NH$_4$VO$_3$
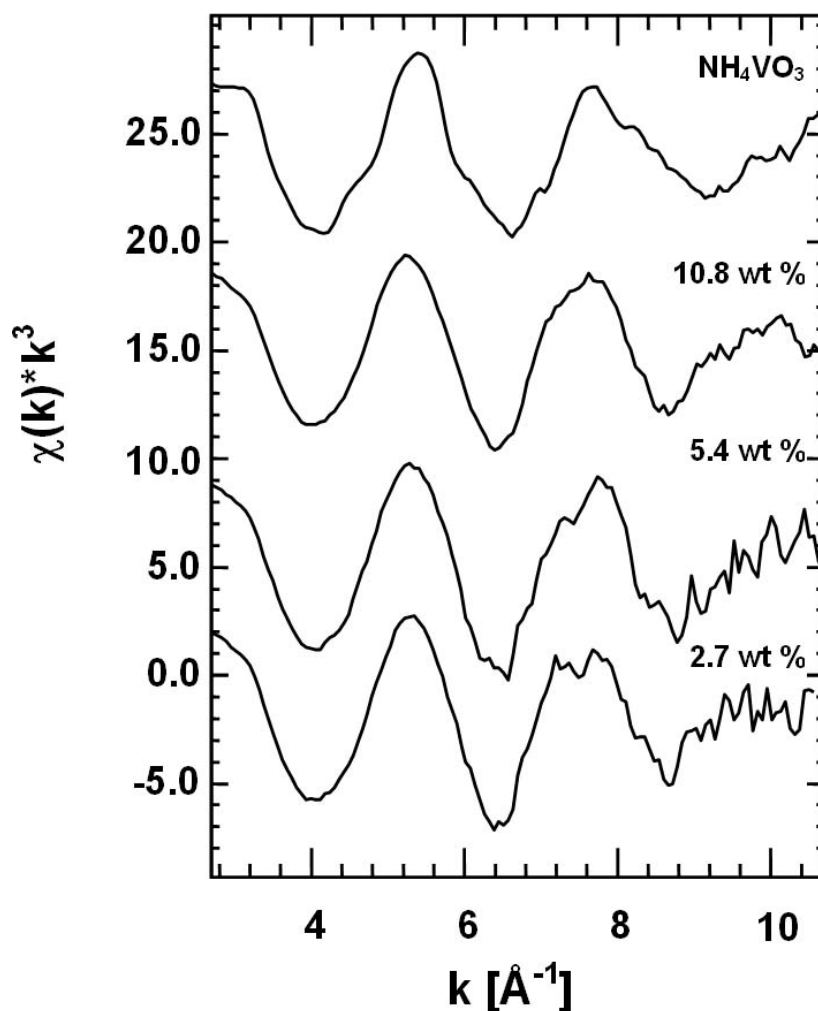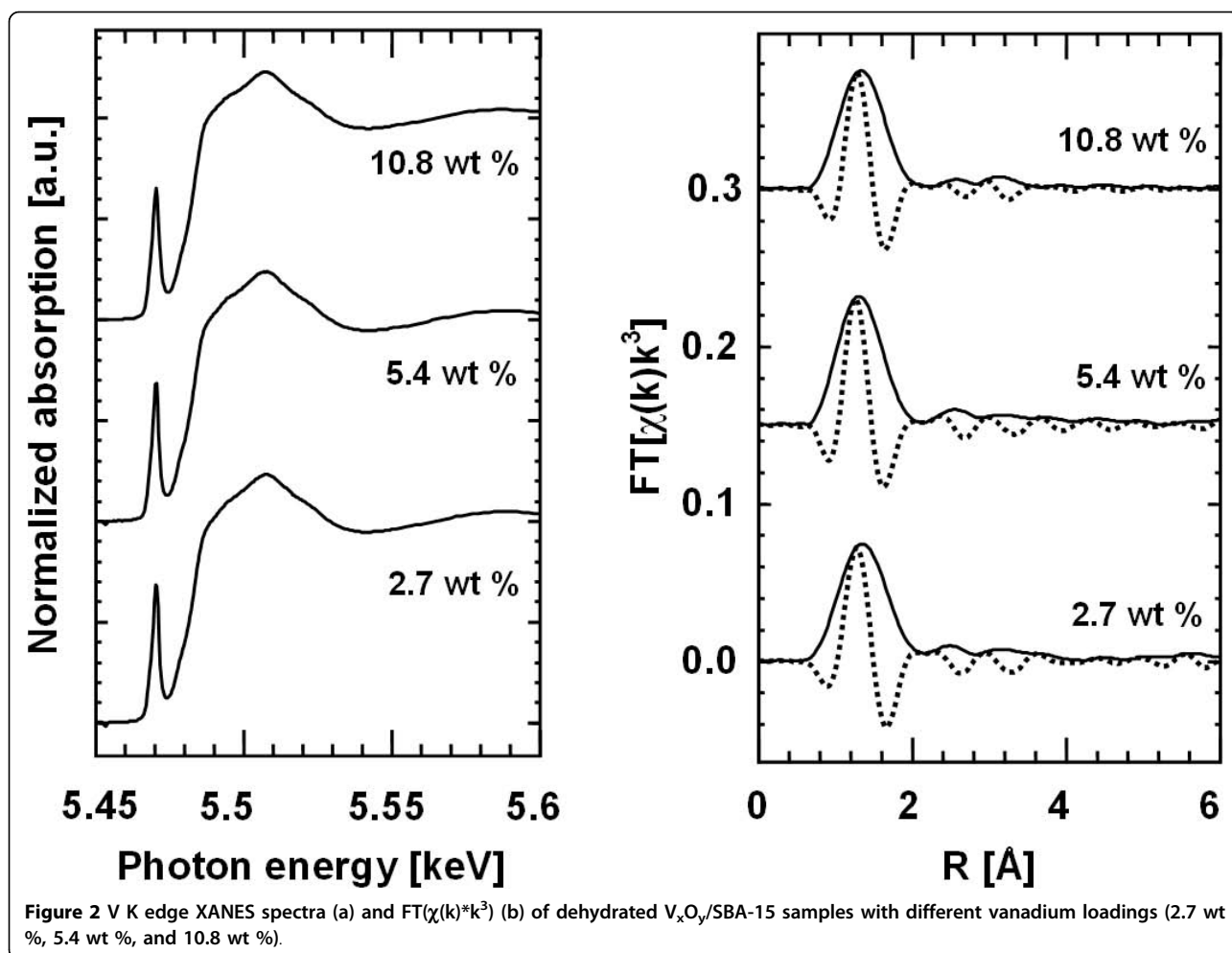

Figure 1 V K edge χ(k) of dehydrated V$_x$O$_y$/SBA-15 with different vanadium loadings (2.7 wt %, 5.4 wt %, and 10.8 wt %) and reference NH$_4$VO$_3$.

Figure 2 V K edge XANES spectra (a) and FT(χ(k)*k^3) (b) of dehydrated V$_x$O$_y$/SBA-15 samples with different vanadium loadings (2.7 wt %, 5.4 wt %, and 10.8 wt %).

and Mg$_2$V$_2$O$_7$ have been identified as suitable references to serve as model systems for a more detailed structural analysis.

Before we discuss the details of analyzing the XAFS data of dehydrated V$_x$O$_y$/SBA-15, a suitable analysis procedure for the higher V-V contributions in the XAFS spectra of references NH$_4$VO$_3$ and Mg$_2$V$_2$O$_7$ was sought. As an example and to reduce the number of tables here, the application of confidence limits and F parameter to distinguish analysis fitting procedures is described for two refinements of a suitable model structure to the experimental FT(χ (k)*k^3)of dehydrated V$_x$O$_y$/SBA-15. The model structure consisted of a tetrahedral coordination of the V center by four oxygen atoms at ~1.7 Å (NH$_4$VO$_3$), two vanadium atoms at distances at ~3.4 Å (NH$_4$VO$_3$) and 3.6 Å (Mg$_2$V$_2$O$_7$), one oxygen atom at ~2.9 Å (Mg$_2$V$_2$O$_7$), and one Si atom at ~2.8 Å (Table 2). Experimental FT(χ(k)*k^3) of Mg$_2$V$_2$O$_7$ and NH$_4$VO$_3$ and the corresponding XAFS refinements are shown in Figure 4. Deviations between the theoretical and experimental spectrum of Mg$_2$V$_2$O$_7$ in the range

from 2 - 4 Å are caused by the number of Mg neighbors and nearly linear multiple-scattering paths in Mg$_2$V$_2$O$_7$ that contribute in this range. These are not sufficiently accounted for by the simplified refinement procedure. The results of the XAFS refinement for dehydrated V$_x$O$_y$/SBA-15, NH$_4$VO$_3$, and Mg$_2$V$_2$O$_7$ are summarized in Table 2. Apparently, the distorted VO$_4$ tetraeder in NH$_4$VO$_3$ required two different V-O distances to be included in the refinement, while Mg$_2$V$_2$O$_7$ and dehydrated V$_x$O$_y$/SBA-15 exhibited a similar single V-O distance. It seems that the distortion in the VO$_4$ units of crystalline reference Mg$_2$V$_2$O$_7$ could not be resolved by the XAFS analysis procedure employed. Accordingly, a lower σ^2 was obtained (0.0012 Å^2) for NH$_4$VO$_3$ compared to those of dehydrated V$_x$O$_y$/SBA-15 and Mg$_2$V$_2$O$_7$ (0.0075 Å^2 and 0.0059 Å^2, respectively). Contrarily, a single V-V distance at 3.47 Å (CN = 2) sufficed for NH$_4$VO$_3$ (consisting of chains of VO$_4$ units), while two V-V distances had to be included for Mg$_2$V$_2$O$_7$ (consisting of adjacent V$_2$O$_7$ units) and dehydrated V$_x$O$_y$/SBA-15. In all three cases, a similar σ^2 parameter
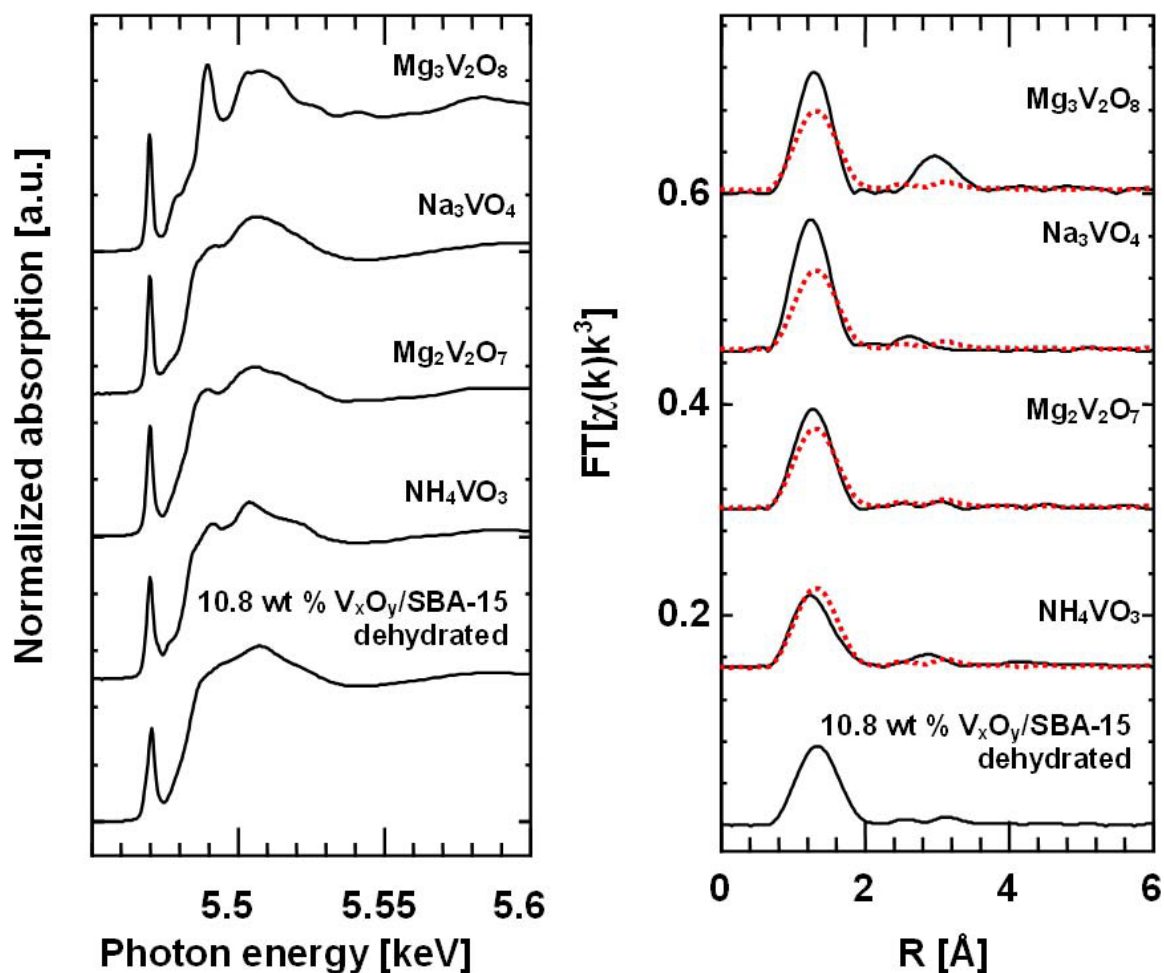
Figure 3 V K edge XANES spectra (a) and FT(χ(k)*k^3) (b) of dehydrated V_xO_y/SBA-15 (10.8 wt %) (dashed on right side) compared to those of various references (i.e. NH_4VO_3, $Mg_2V_2O_7$, Na_3VO_4, and $Mg_3V_2O_8$).

Table 2 EXAFS refinement results obtained for experimental FT(χ(k)*k^3) of dehydrated V_xO_y/SBA-15, NH_4VO_3, and $Mg_2V_2O_7$.

| | Model | | V_xO_y-SBA-15 | | $Mg_2V_2O_7$ | | NH_4VO_3 | |
Type	N	R [Å]	R [Å]	σ^2 [Å^2]	R [Å]	σ^2 [Å^2]	R [Å]	σ^2 [Å^2]
V-O	1	1.63	1.78	0.0075	1.74	0.0059	1.68	0.0012
V-O	1	1.70	1.78$_C$	0.0075$_C$	1.74$_C$	0.0059$_C$	1.68$_C$	0.0012$_C$
V-O	2	1.76	1.78$_C$	0.0075$_C$	1.74$_C$	0.0059$_C$	1.84	0.0012$_C$
V-O	1	2.87	2.89	0.0017	2.77	0.0165	-	-
V-V	1	3.36	3.30	0.0135	3.28	0.0134	3.47	0.0147
V-V	1	3.62	3.62	0.0135$_C$	3.56	0.0134$_C$	3.47$_C$	0.0147$_C$
V-Si	1	2.80	2.54	0.0121	-	-	-	-

Type and number (N) of atoms at distance R from the absorbing V atom in a model system assuming an ordered arrangement of V_2O_7 units (Figure 7) compared to experimental distances and XAFS disorder parameters (σ^2). Parameters were obtained from the refinement of this model structure to the experimental V K edge XAFS FT(χ(k)*k^3) of dehydrated V_xO_y/SBA-15 (10.8 wt %), $Mg_2V_2O_7$, and NH_4VO_3 (k range from 2.7-11.0 Å^{-1}, R range 0.8-4.0 Å, N_{ind} = 18, E_0 = 0 eV in all cases, fit residual 3.6 (dehydrated V_xO_y/SBA-15) (N_{free} = 9), 11.2 ($Mg_2V_2O_7$) (N_{free} = 7), 8.9 (NH_4VO_3) (N_{free} = 5)) (Subscript C indicates parameters that were correlated in the refinement). Confidence limits and significance of fitting parameters are given in Table 3.

for the V-V contributions of about 0.014 Å^2 was obtained.

The corresponding confidence limits and significance parameters F are given in Table 3. In fitting procedure #1 two V-O distances in the first V-O shell were allowed to vary independently (both with a CN of 2 and the same σ^2). Moreover, E_0 was also allowed to vary in fitting procedure #1. Because of N_{ind} = 18 and N_{free} = 11 refinement procedure #1 would be taken as reliable according to the Nyquist criteria. However, confidence limits of the first V-O distance of ± 0.1 Å and an F parameter of 0.7 for both distance and σ^2 were obtained with procedure #1. Moreover, E_0 exhibited a confidence limit of ± 9.2 and F = 0.9. Apparently, fitting procedure #1 already exceeds the number of meaningful parameters and yield ambiguous structural parameters. On the one hand, the reduced amplitude of the FT(χ(k)*k^3) of dehydrated V_xO_y/SBA-15 compared to that of references consisting of undistorted VO_4 units (Figure 3) suggested the presence of more than
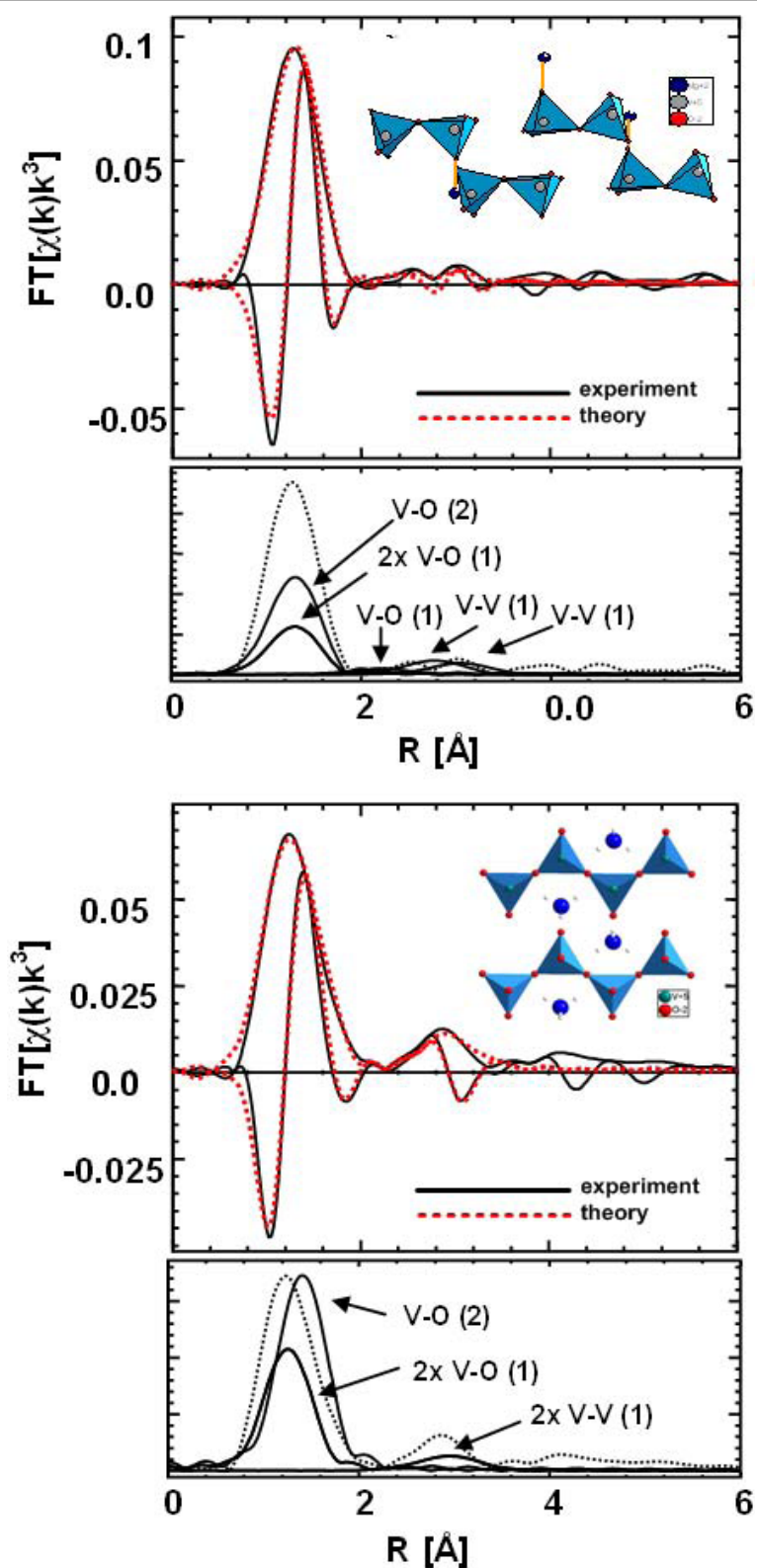
Figure 4 Experimental (solid) V K edge FT(χ(k)*k^3) of NH$_4$VO$_3$, Mg$_2$V$_2$O$_7$ reference together with a theoretical XAFS function (fitting results are given in Table 2). Also shown are the Fourier transformed χ(k)*k^3 of the individual scattering paths together with corresponding coordination number in brackets. brackets.

Table 3 Evaluation of EXAFS refinement of dehydrated V_xO_y/SBA-15.

Type R [Å] σ^2 [Å^2]		Procedure #1			Procedure #2		
	N	Z	± z	F	Z	± z	F
R(V-O)	4(2)	1.81	0.11	0.7	1.78	0.005	0
σ^2(V-O)	4	0.0066	0.0047	0.7	0.0075	0.0004	0
R(V-O)	-(2)	1.75	0.04	0.4	-	-	
R(V-O)	1	2.89	0.01	0.5	2.90	0.011	0
σ^2(V-O)	1	0.0014	0.0017	0.9	0.0017	0.0018	0.7
R(V-V)	1	3.29	0.017	0	3.29	0.016	0
σ^2(V-V)	2	0.0135	0.0203	0.7	0.0135	0.00035	0.3
R(V-V)	1	3.61	0.019	0	3.62	0.024	0
R(V-Si)	1	2.54	0.01	0	2.54	0.011	0
σ^2(V-Si)	1	0.0115	0.0011	0.3	0.0121	0.0011	0
E_0	-	-0.9	-0.3	0.8	-	-	-

V K edge XAFS parameters (Z for distances R and disorder parameter σ^2) obtained from two different procedures of fitting a model structure (i.e. "ordered V_2O_7 dimers" on SiO_2 support) to the experimental XAFS FT(χ(k)*k^3) of dehydrated V_xO_y/SBA-15 (10.8 wt %) (details of fit given in Table 2) together with confidence limits (± z, referring to 95% of fit residual) and significance parameters F (details given in text). Fit residual 3.1 for Procedure #1 and 3.6 for Procedure #2.

one V-O distance, including a short "vanadyl" V = O distance. On the other hand, however, the resolution in the experimental FT(χ(k)*k^3) and the available degree of freedom did not permit refining more than one V-O distance in the procedure used. Therefore, the fitting procedure was modified. In the following, E_0 was kept invariant in the refinement and only one V-O distance at ~1.75 Å was used. In contrast to procedure #1, procedure #2 yielded reasonable confidence limits and acceptable F parameters.

The σ^2 parameter of the V-O contribution at 2.9 Å exhibited a rather high confidence limit and F = 0.7. Apparently, both V-O and V-Si neighbors in the distance range from 2.5 Å to 2.9 Å are required for a good refinement of the model structure to the experimental data. This is indicated by the confidence limits and F parameters calculated for the corresponding distances (Table 3). Nevertheless, the high σ^2 obtained for the V-Si contribution and the rather low σ^2 obtained for the V-O at 2.9 Å indicate a certain ambiguity of the corresponding fitting results. The reason may be a considerable static disorder and, thus, a broadened V-Si distance distribution. Hence, calculating and evaluating confidence limits and F tests permitted to arrive at a meaningful and reliable fitting procedure. In that, the approach employed appears to be superior to only calculating the Nyquist criteria. In total, procedure #2 worked very well for XAFS data analysis of dehydrated V_xO_y/SBA-15 and $Mg_2V_2O_7$. In contrast, the local structure around V centers in NH_4VO_3 was best described by assuming two different V-O distances in the first coordination shell and only one

V-V distance at 3.47 Å (CN = 2) (Table 2). A V-O distance at 2.8 Å was found to be insignificant.

Local structure of dehydrated V_xO_y/SBA-15 - XAFS refinement of "VO$_4$" based model structures

After having identified two suitable references as model structures for XAFS refinements to the experimental FT (χ(k)*k^3) of dehydrated V_xO_y/SBA-15 (Figure 3(b)), the XAFS analysis approach chosen shall be described in more detail. In addition to using confidence limits and F tests as introduced above, the suitable XAFS fitting procedure was developed stepwise as outlined in the following.

First, we started with an often repeated assumption from the literature. DR-UV-Vis or Raman measurements revealed that dehydration of V_xO_y/SBA-15 resulted in a characteristic change from a distorted square pyramidal to a distorted tetrahedral coordination [10,13,16]. The local structure of vanadium oxide species supported on SiO_2 was assumed to correspond to isolated VO$_4$ units. Hence, in a first *tetrahedron approach* the theoretical XAFS function of a VO$_4$ tetrahedron consisting of two slightly different V-O distances was refined to the FT(χ(k)*k^3) of dehydrated V_xO_y/SBA-15 (Figure 5, top) together with the Fourier transformed χ(k)*k^3 of the individual scattering paths). Because of the similar height of the pre-edge peak in the XANES (Figure 3(a)) and the first V-O peak in the FT(χ(k)*k^3), phases and amplitudes employed in the refinement were calculated using the model structure of NH_4VO_3 (ICSD 1487 [26]) and $Mg_2V_2O_7$ (ISCD 2321 [27]). Figure 5, top shows a good agreement between theoretical and experimental FT(χ(k)*k^3) of dehydrated V_xO_y/SBA-15 for the first V-O peak below 2 Å. Naturally, the amplitude between 2 Å and 4 Å in the FT(χ(k)*k^3) could not be accounted for. Hence, a structural model assuming only isolated VO$_4$ species cannot adequately describe the local structure around the V centers in dehydrated V_xO_y/SBA-15.

Therefore, we assumed that higher coordination shells around the vanadium centers significantly contribute to the FT(χ(k)*k^3) of dehydrated V_xO_y/SBA-15. These shells have to be included in the refinement. A seemingly expected contribution may arise from silicon backscatterers in the SiO_2 support at distances of less than 3.0 Å. This has been previously proposed by Keller et al. [20]. Thus, in extension of the *tetrahedron approach* a silicon atom at a V-Si distance of 2.8 Å was included in the theoretical model. In the corresponding "O_3V-O-Si" unit a Si-O distance of 1.62 Å is assumed (inset in Figure 5, bottom)), as it is found in various silicates. The result of the XAFS refinement of the "O_3V-O-Si" model to the FT(χ(k)*k^3) of dehydrated V_xO_y/SBA-15 is depicted in Figure 5, bottom). The additional Si backscatterer resulted in a better agreement between theoretical and
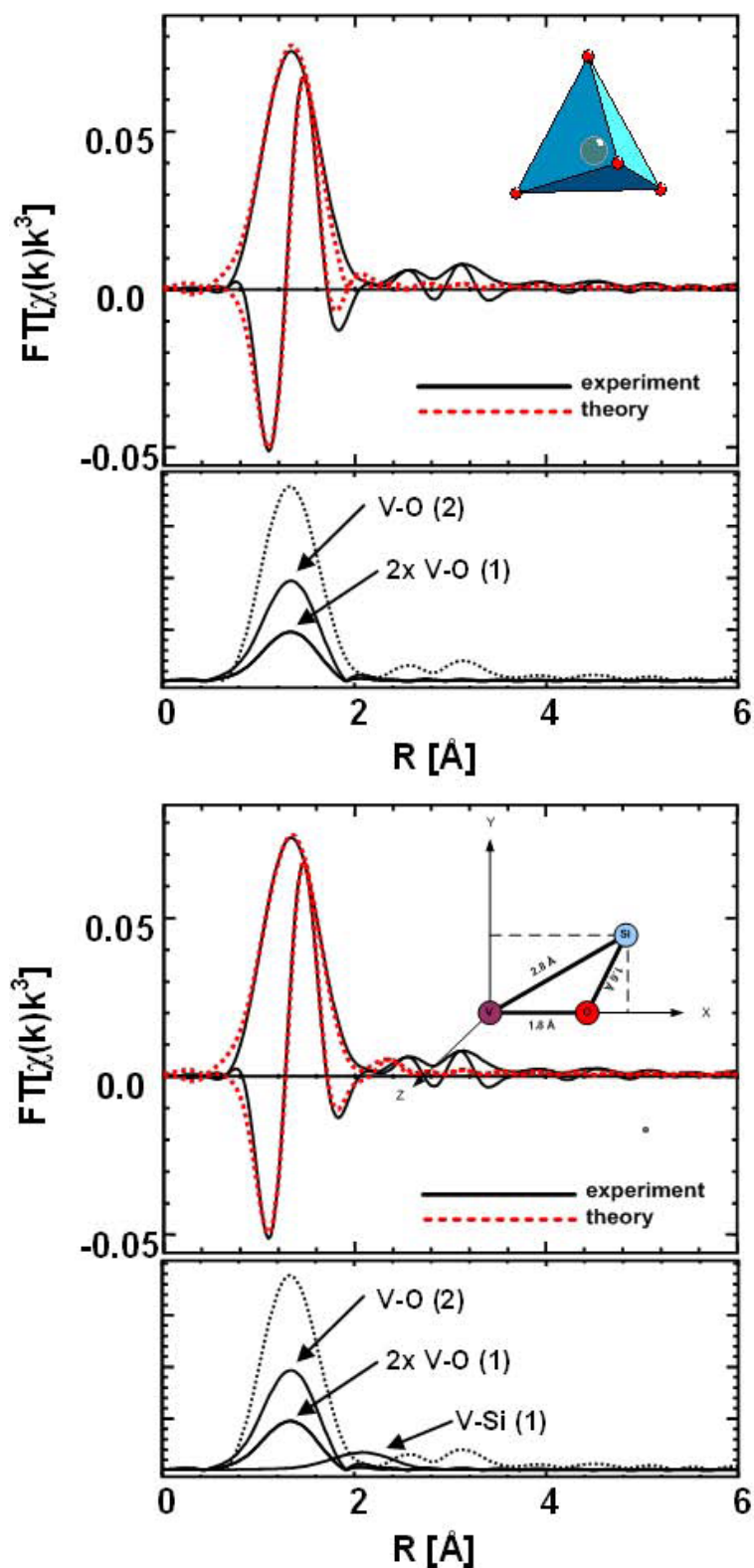
Figure 5 Experimental (solid) V K edge FT(χ(k)*k^3) of dehydrated V_xO_y/SBA-15 (10.8 wt %) together with theoretical XAFS functions (top: "isolated VO$_4$" model, bottom: addition of V-Si path to "isolated VO$_4$" model). Insets show the VO$_4$ tetrahedron (top) and a schematic representation of the V-Si path employed (bottom). Also shown are the Fourier transformed χ(k)*k^3 of the individual scattering paths together with corresponding coordination number in.

experimental FT(χ(k)*k^3) at distances of about 2.4 Å (not phase shift corrected). The resulting V-Si distance amounted to 2.54 Å, comparable to the distance obtained by Keller et al. (2.61 Å [20]). However, it can be easily seen from Figure 5, bottom) that the amplitude in the FT(χ(k) *k^3) of dehydrated V$_x$O$_y$/SBA-15 between 2.4 and 4.0 Å is still not accounted for.

Local structure of dehydrated V$_x$O$_y$/SBA-15 - XAFS refinement of "V$_2$O$_7$" based model structures

Figure 5 shows that an "isolated VO$_4$" model did not properly describe the local structure between 2 Å and 4 Å around vanadium centers in dehydrated V$_x$O$_y$/SBA-15. Hence, we assumed that at least "V$_2$O$_7$ dimers" would be needed to achieve a good agreement between theoretical and experimental XAFS FT(χ(k)*k^3). V$_2$O$_7$ units are present in the structures of the references NH$_4$VO$_3$ and Mg$_2$V$_2$O$_7$ whose spectra resembled best the XANES and EXAFS spectra of dehydrated V$_x$O$_y$/

SBA-15 (Figure 3). Therefore, a V-V scattering path at 3.4 Å was included in the model used in the XAFS refinement. This distance corresponds to the shortest V-V distance between two corner-sharing VO$_4$ tetrahedrons in "V$_2$O$_7$ dimers" of NH$_4$VO$_3$ and Mg$_2$V$_2$O$_7$. The result of the corresponding XAFS refinement is shown in. Apparently, a structural model based on isolated V$_2$O$_7$ dimers was equally unsuited to describe the local structure around V centers in dehydrated V$_x$O$_y$/SBA-15. The agreement between theoretical and experimental FT(χ(k)*k^3) in the range from 2 to 4 Å is still not sufficient (Figure 6). Also, adding a V-Si distance to this "isolated V$_2$O$_7$ dimer model" only resulted in a minor improvement of the refinement.

Figure 5 and Figure 6 clearly show that neither an "isolated VO$_4$" model nor an "isolated V$_2$O$_7$" model properly describe the local structure of the majority of V centers in dehydrated V$_x$O$_y$/SBA-15. Hence, in the next step an ordered arrangement of neighboring V$_2$O$_7$
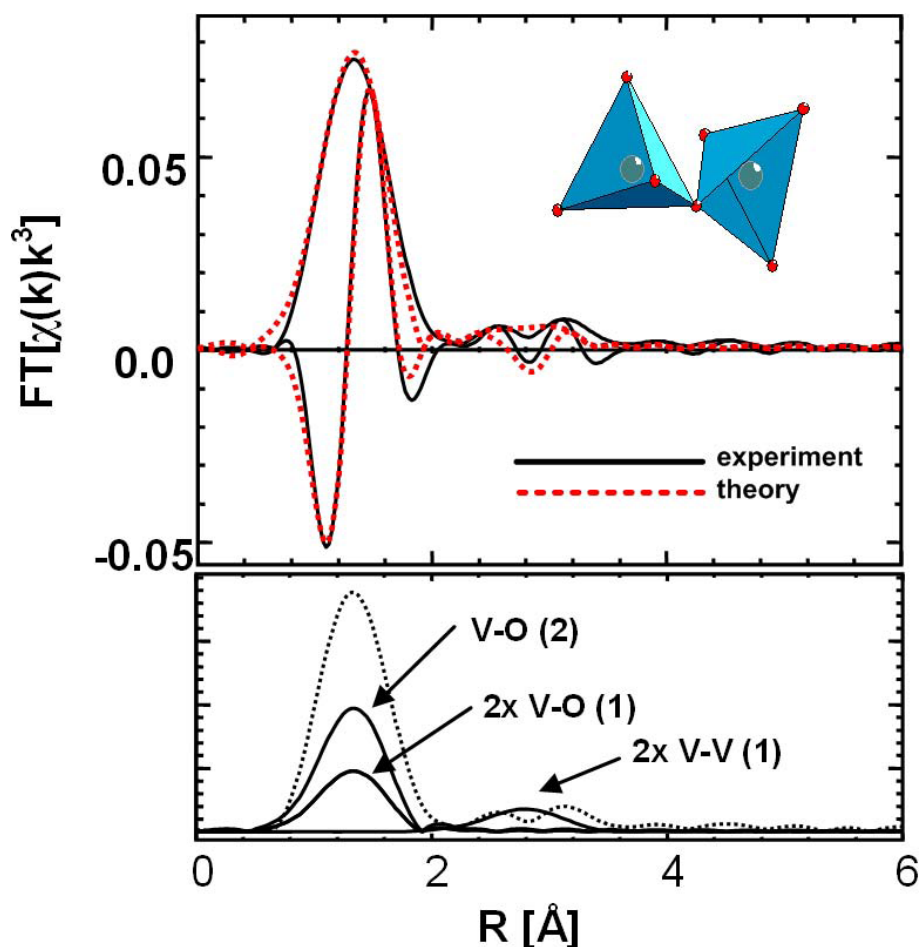

Figure 6 Experimental (solid) V K edge FT(χ(k)*k^3) of dehydrated V$_x$O$_y$/SBA-15 (10.8 wt %) together with a theoretical XAFS function (i.e. "isolated V$_2$O$_7$" model). Inset shows the V$_2$O$_7$ dimer. Also shown are the Fourier transformed χ(k)*k^3 of the individual scattering paths together with corresponding coordination number in brackets.

units was assumed. Because of their similar XANES and EXAFS spectra, we again referred to NH_4VO_3 and $Mg_2V_2O_7$ as references. V_2O_7 units form chains in NH_4VO_3 with one V-V distance. Conversely, V_2O_7 units are neighboring but more separated in $Mg_2V_2O_7$ resulting in two distinct V-V distances (ICSD 2321 [27]). Accordingly, two additional scattering paths were added to the previous "isolated V_2O_7" model. These two paths correspond to V-O (2.8 Å) and V-V (3.6 Å) distances between two neighboring V_2O_7 units in the structure of $Mg_2V_2O_7$. The result of the corresponding XAFS refinement to the $FT(\chi(k)*k^3)$ of dehydrated V_xO_y/SBA-15 is shown in Figure 7 together with the various V-O and V-V distances used. Apparently, assuming neighboring V_2O_7 units in an ordered arrangement supported on SBA-15 yielded a good agreement between theoretical and experimental $FT(\chi(k)*k^3)$ of dehydrated V_xO_y/SBA-15 over the extended R range from 1 Å to 4 Å. The structural and fitting parameters obtained from the XAFS refinement to the experimental $FT(\chi(k)*k^3)$ of dehydrated V_xO_y/SBA-15 and $Mg_2V_2O_7$ are given in Table 2. The similar V-O distances, V-V distances, and σ^2 parameters of dehydrated V_xO_y/SBA-15 and $Mg_2V_2O_7$ corroborate our choice of model system to describe the local structure around V centers dehydrated V_xO_y/SBA-15.

Schematic structural representation of dehydrated V_xO_y/SBA-15

A schematic structural representation of the ordered arrangement of V_2O_7 units in dehydrated V_xO_y/SBA-15 is depicted in Figure 8. In contrast to previous results on low loaded (< 1 V/nm^2) V_xO_y/SiO$_2$ samples [17,21] we conclude that isolated VO$_4$ units are not the major vanadium oxide species present on the dehydrated V_xO_y/SBA-15 samples studied here. From the different loadings studied, only the 2.7 wt % V_xO_y/SBA-15 sample possessed a vanadium content of less than 1 V/nm^2. The three dehydrated V_xO_y/SBA-15 samples exhibited only minor differences in their XANES spectra (Figure 2), FT $(\chi(k)*k^3)$ (Figure 9), and XAFS fitting results (Table 4). Hence, independent of the V loading in the range 2.7 - 10.8 wt % the local structure of the majority of V centers in dehydrated V_xO_y/SBA-15 is described best by an ordered arrangement of neighboring V_2O_7 units (Table 4, Figure 9). Decomposition of the decavanadate precursor during calcinations of the as-prepared materials will most likely result in the formation of dehydrated V_xO_y/SBA-15. Any description of the formation mechanism of ordered V_2O_7 units on the surface of SiO$_2$, however, is beyond the scope of this work. Exposure of the calcined material to ambient conditions apparently results in re-hydration and formation of the hydrated V_xO_y species supported on SBA-15. This transformation already

suggests a reversible hydration-re-hydration behavior of vanadium oxide species supported on SBA-15 which should be the subject of further studies.

The presence of non-monomeric V_xO_y species in dehydrated V_xO_y/SBA-15 samples was also recently concluded based on NEXAFS studies combined with theoretical calculations [28]. Eventually, structural evolution and catalytic activity of dehydrated V_xO_y/SBA-15 were studied by combined in situ XAS-MS under selective propene oxidation reaction condition. Onset of catalytic activity was detected at about 573 K. The in situ XAS data measured indicated, that the characteristic ordered arrangement of V_2O_7 dimers in the local structure of dehydrated V_xO_y/SBA-15 persisted under catalytic reaction conditions. A more detailed analysis of structure activity correlations of V_xO_y/SBA-15 under selective oxidation reaction conditions will be presented elsewhere.

Oxygen and silicon atoms of the SiO$_2$ support are not depicted in the schematic representation depicted in Figure 8. In particular Si atoms in the topmost layer of SiO$_2$ belong to the second coordination sphere of the V centers. Previous reports have indicated that V-Si distances may contribute to the experimental $FT(\chi(k)*k^3)$ of dehydrated V_xO_y/SBA-15 [19]. Therefore, a single V-Si scattering path was included in the refinement of the "neighboring V_2O_7" model described above (Figure 7). The structural parameters and refinement details are given in Table 2 and Table 4. Comparing fit residuals, confidence limits, and F parameters a significant improvement was visible. Apparently, both local structure in V_xO_y species and interaction with SiO$_2$ support are required to describe the $FT(\chi(k)*k^3)$ of dehydrated V_xO_y/SBA-15 samples.

Limitations of XAFS analysis of dehydrated V_xO_y/SBA-15

Eventually, the limitations of the XAFS analysis of dehydrated V_xO_y/SBA-15 presented here should be discussed. XAFS is not a very sensitive technique with respect to distinguishing and identifying additional minority species. Experimental XAFS spectra are clearly dominated by the signal of the majority phase. Hence, the presence of minority vanadium oxide species in dehydrated V_xO_y/SBA-15 with concentrations of less than ~5% cannot be excluded. Only if the contribution of additional phases amounts to more than ~5-10%, distortion of the $FT(\chi(k)*k^3)$ and deviation from the model structure assumed will be detectable. This holds in particular, if these minority species happen to be less ordered than the majority phase.

Moreover, XAFS is an averaging technique. Certainly, higher shells should be properly taken into account and various references should be measured for comparison. Even then, however, it may remain difficult to unambiguously distinguish between mixtures of various
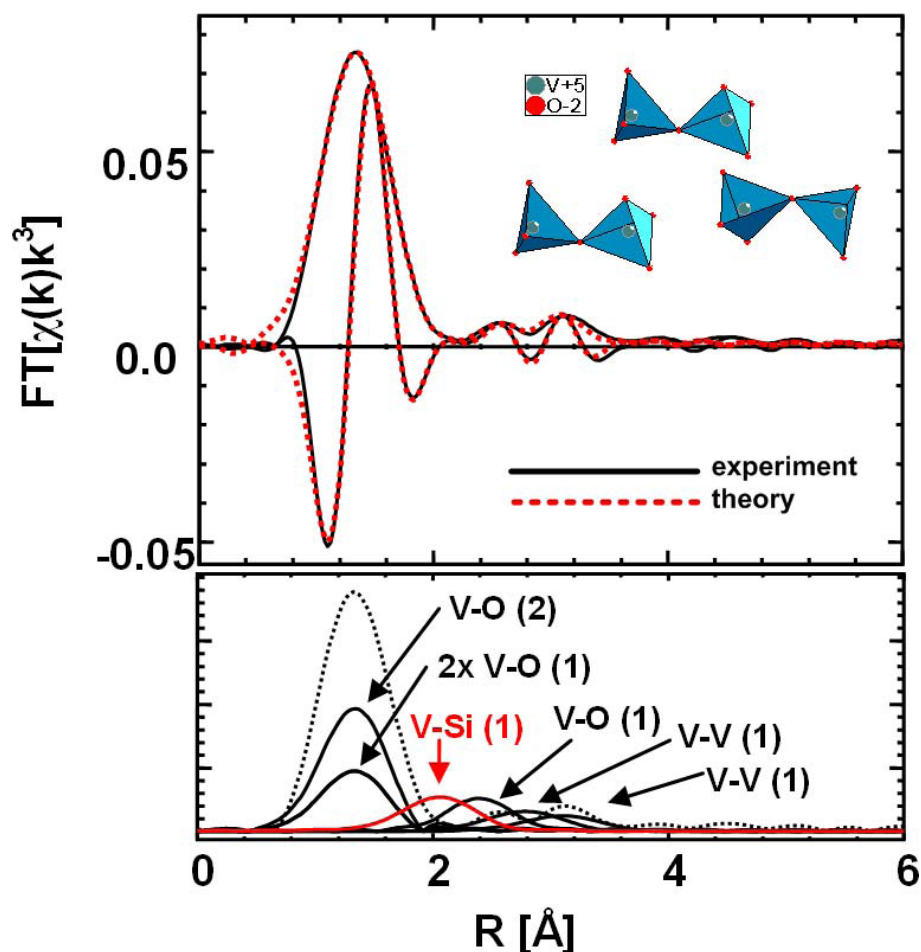
Figure 7 Experimental (solid) V K edge FT(χ(k)*k^3) of dehydrated V$_x$O$_y$/SBA-15 (10.8 wt %) together with a theoretical XAFS function (i.e. "ordered arrangement of V$_2$O$_7$" model). Fitting results are given in Table 2. Inset shows a schematic representation of arrangement of V$_2$O$_7$ units in Mg$_2$V$_2$O$_7$. Also shown are the Fourier transformed χ(k)*k^3 of the individual scattering paths together with corresponding coordination number in brackets.
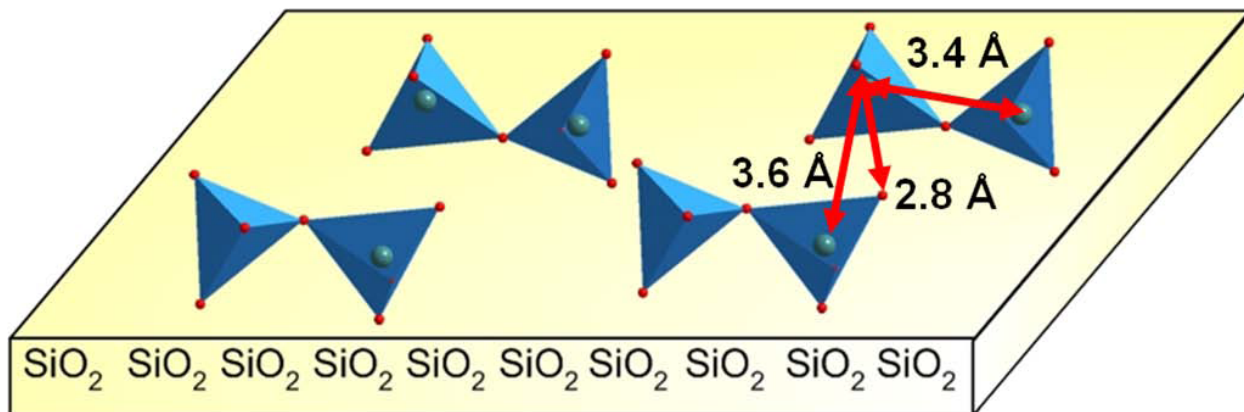

Figure 8 Schematic structural representation of dehydrated V$_x$O$_y$/SBA-15. The most prominent distances employed in the XAFS refinement procedure are indicated.
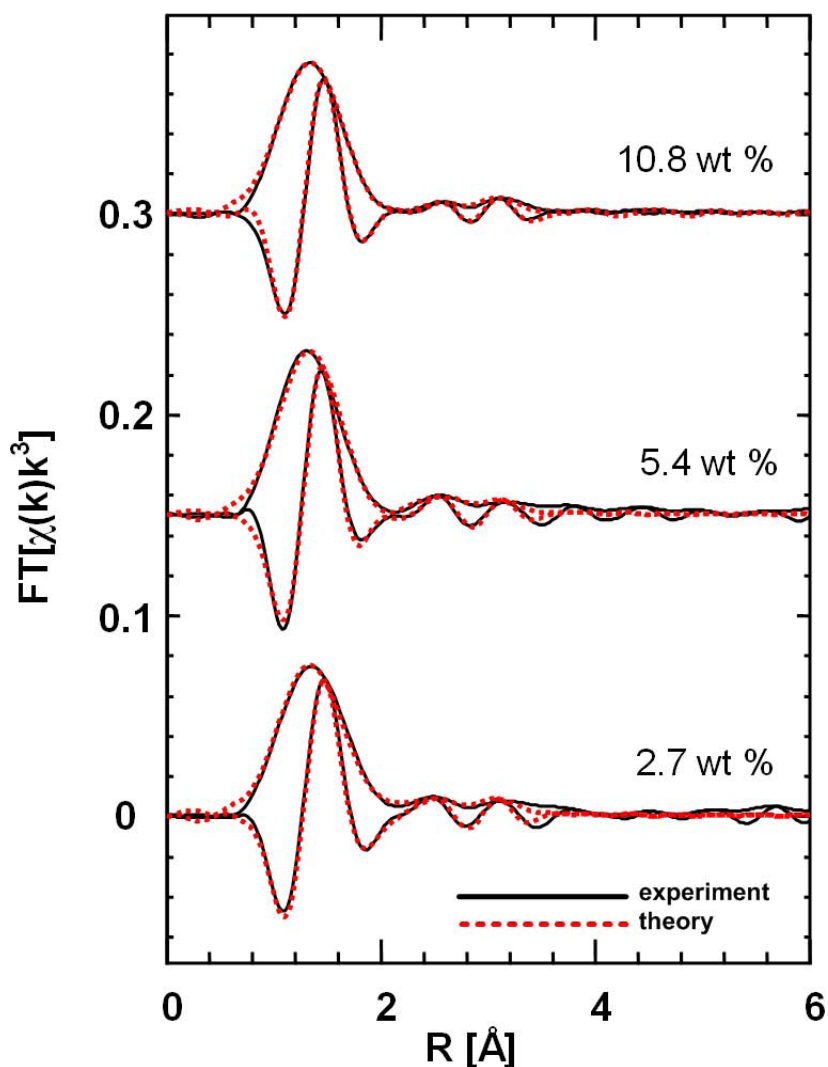
Figure 9 Experimental (solid) V K edge FT(χ(k)*k^3) of dehydrated V$_x$O$_y$/SBA-15 (2.7 wt %, 5.4 wt %, and 10.8 wt %) together with a theoretical XAFS function (structural model depicted in Figure 7). Fitting results are given in Table 4.

Table 4 EXAFS refinement results obtained for different V loadings on V$_x$O$_y$/SBA-15 in the dehydrated state.

	Model		10.8 wt %		5.4 wt %		2.7 wt %	
Type	N	R [Å]	R [Å]	σ^2[Å^2]	R [Å]	σ^2[Å^2]	R [Å]	σ^2[Å^2]
V-O	1	1.63	1.78	0.0075	1.77	0.0069	1.78	0.0075
V-O	1	1.70	1.78	0.0075	1.77	0.0069	1.78	0.0075
V-O	2	1.76	1.78	0.0075	1.77	0.0069	1.78	0.0075
V-V	1	3.36	3.30	0.0135	3.33	0.0114	3.37	0.0113
V-O	1	2.87	2.90	0.0017	2.87	0.0022	2.86	0.0015
V-V	1	3.62	3.62	0.0135	3.62	0.0114	3.65	0.0113
V-Si	1	2.80	2.54	0.0121	2.53	0.0139	2.54	0.0081

Type and number (N) of atoms at distance R from the absorbing V atom in a model system assuming an ordered arrangement of V$_2$O$_7$ units (Figure 7) compared to experimental distances and XAFS disorder parameter (σ^2). Parameters were obtained from the refinement of this model structure to the experimental V K edge XAFS FT(χ(k)*k^3) of dehydrated V$_x$O$_y$/SBA-15 with different V loadings (i.e. 10.8 wt %, 5.4 wt %, 2.7 wt %) (Figure 9) (k range from 2.7-11.0 Å^{-1}, R range 0.8-4.0 Å, N$_{ind}$ = 18, N$_{free}$ = 9, E$_0$ = 0 eV in all cases, fit residual 3.6 (10.8 wt %), 7.0 (5.4 wt %), 7.8 (2.7 wt %)) (Subscript C indicates parameters that were correlated in the refinement). Confidence limits and significance of fitting parameters correspond to those given in for the 10.8 wt % sample.

species or structures. Hence, alternative scenarios with different vanadium oxide species need to be considered and discussed. An equal mixture of isolated VO_4 and neighboring V_2O_7 units, for instance, may exhibit a XAFS $FT(\chi(k)*k^3)$ similar to that presented here. For two reasons this assumption is not very likely. First, the V-O distances in the first "VO_4" shell of the two species would have to be the same. Otherwise a strong reduction in amplitude of the first V-O peak in the $FT(\chi(k)*k^3)$ caused by destructive interference would be discernible. Second, isolated VO_4 would not contribute to the $FT(\chi(k)*k^3)$ in the range from 2 Å to 4 Å. Thus, reduction in amplitude and much higher σ^2 parameters compared to reference $Mg_2V_2O_7$ would be detectable. Both are not observed in the EXAFS analysis of dehydrated V_xO_y/SBA-15 presented here (Figure 3(b), Table 2). A similar statement holds for isolated V_2O_7 units or a less ordered arrangement of neighboring V_2O_7 units. Both would result in a reduction in $FT(\chi(k)*k^3)$ amplitude because of missing contribution in the 2-4 Å range or destructive interference caused by a broadened distribution of distances, respectively. Moreover, for isolated or less ordered V_2O_7 units a single V-V distance would suffice to describe the experimental XAFS spectrum. This was also not observed in the XAFS analysis procedure employed. Eventually, higher V-Si distances may have to be considered in addition to a V-Si distance of ~2.5 Å (Table 2). However, a significant contribution of V-Si distances at more 3.0 Å range in the $FT(\chi(k)*k^3)$ would require a highly ordered arrangement of V_xO_y species on the SiO_2 support and a very narrow distance distribution. This seems to be unlikely.

In total, assuming a structural arrangement of vanadium centers in dehydrated V_xO_y/SBA-15 that has already been established for reference vanadium oxides (i.e. $Mg_2V_2O_7$) is simple and results in a good agreement with experimental data. More complex and artificially constructed arrangements of V_xO_y species supported on SiO_2 may be conceivable but appear to be less likely. Both XANES and EXAFS analysis corroborate a local structure around the majority of V centers in dehydrated V_xO_y/SBA-15 similar to the ordered arrangement of neighboring V_2O_7 dimers in the structure of $Mg_2V_2O_7$.

Local structure of hydrated V_xO_y/SBA-15 Comparison to V oxide references

The EXAFS $\chi(k)*k^3$ of hydrated V_xO_y/SBA-15 (as-prepared) with different V loadings are depicted in Figure 10. The usable spectral ranged extended from 2.7 Å through 10.5 Å. The V K edge XANES spectra and the $FT(\chi(k)*k^3)$ of hydrated V_xO_y/SBA-15 are shown in Figure 11. The Fourier transformed $\chi(k)*k^3$ and the V K near edge spectra of hydrated V_xO_y/SBA-15 are compared to those of

vanadium oxide references in Figure 12. The XANES spectrum of hydrated V_xO_y/SBA-15 resembles that of MgV_2O_6, $[H_3N(CH_2)_4]_6V_{10}O_{28}$, and V_2O_5 (Figure 12(a)). In these vanadium oxide references vanadium centers exhibit a distorted octahedral or distorted square pyramidal coordination. The XANES spectra of hydrated V_xO_y/SBA-15, V_2O_5, MgV_2O_6, and $[H_3N(CH_2)_4]_6V_{10}O_{28}$ show a similar height of the pre-edge peak. Because the pre-edge peak height is determined by the coordination of the vanadium centers [29], hydrated V_xO_y/SBA-15 also appears to exhibit a distorted square pyramidal coordination of V centers. This has also been observed by Bell et al. [18] and others.

The range of potential model structures describing the local structure of hydrated V_xO_y/SBA-15 can be further narrowed when comparing the corresponding $FT(\chi(k)*k^3)$ (Figure 12(b)). Considering peak positions and relative peak heights in the $FT(\chi(k)*k^3)$, it appears that from the references available the $FT(\chi(k)*k^3)$ of V_2O_5 resembles that of hydrated V_xO_y/SBA-15. Because of the lower intensity in the $FT(\chi(k)*k^3)$ hydrated V_xO_y/SBA-15 may possess a more disordered structure compared to that of crystalline V_2O_5. This is in good agreement with a detailed comparison of the corresponding XANES spectra. On the one hand, the positions of the various peaks in the XANES of hydrated V_xO_y/SBA-15 are similar to that of V_2O_5 (Figure 12(a)). On the other hand, the lower peak intensities are also indicative of a disordered V_2O_5 like structure of the vanadium oxide species in hydrated V_xO_y/SBA-15.

Local structure of hydrated V_xO_y/SBA-15 XAFS refinement of "V_2O_5" based model structure

Comparison of the XANES and $FT(\chi(k)*k^3)$ of hydrated V_xO_y/SBA-15 to those of various references identified V_2O_5 as most suitable model structure for a detailed EXAFS analysis. Ammonium decavanadate decomposes to V_2O_5 during treatment in air at temperatures above 773 K. Calcination of the materials studied here will most likely result in formation of the dehydrated species as described above. Re-hydration upon exposure to ambient conditions resulted in vanadium oxide species supported on SBA-15 with a local structure similar to that of V_2O_5. A detailed discussion of the underlying formation mechanisms is beyond the scope of this work. Therefore, a theoretical XAFS function calculated on the basis of a V_2O_5 model structure (ICSD 60767 [30]) was refined to the experimental $FT(\chi(k)*k^3)$ of hydrated V_xO_y/SBA-15. Details of the XAFS refinement procedure and the structural parameters obtained are given in Table 5. In addition, the V_2O_5 model structure was refined to the $FT(\chi(k)*k^3)$ of V_2O_5 to validate the procedure chosen. Good agreement between the theoretical XAFS function of a V_2O_5 model structure and the
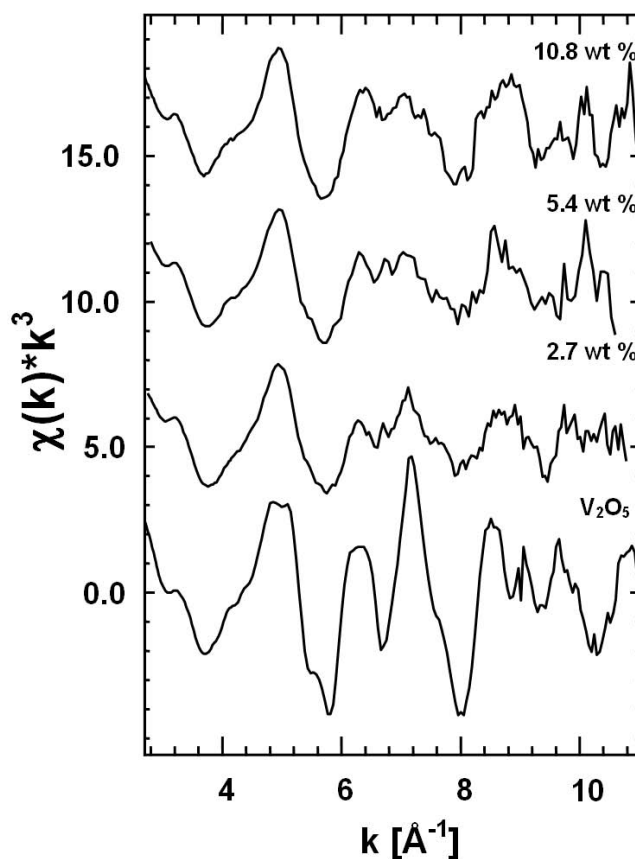
Figure 10 V K edge $\chi(k)$ of hydrated V_xO_y/SBA-15 samples with different vanadium loadings (2.7 wt %, 5.4 wt %, and 10.8 wt %) and reference V_2O_5.
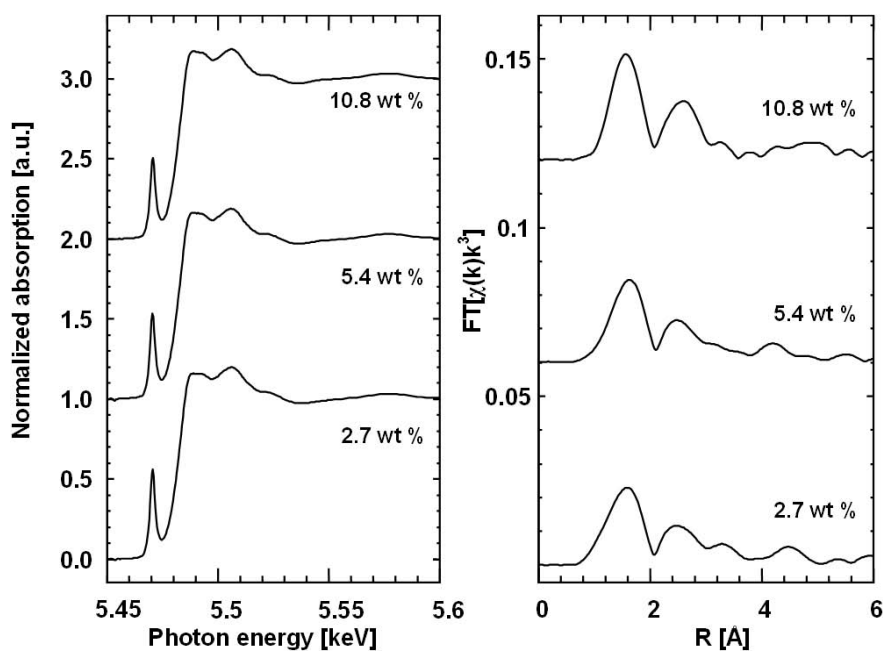
Figure 11 V K edge XANES spectra (a) and FT($\chi(k)*k^3$) (b) of hydrated V_xO_y/SBA-15 samples with different vanadium loadings (2.7 wt %, 5.4 wt %, and 10.8 wt %).
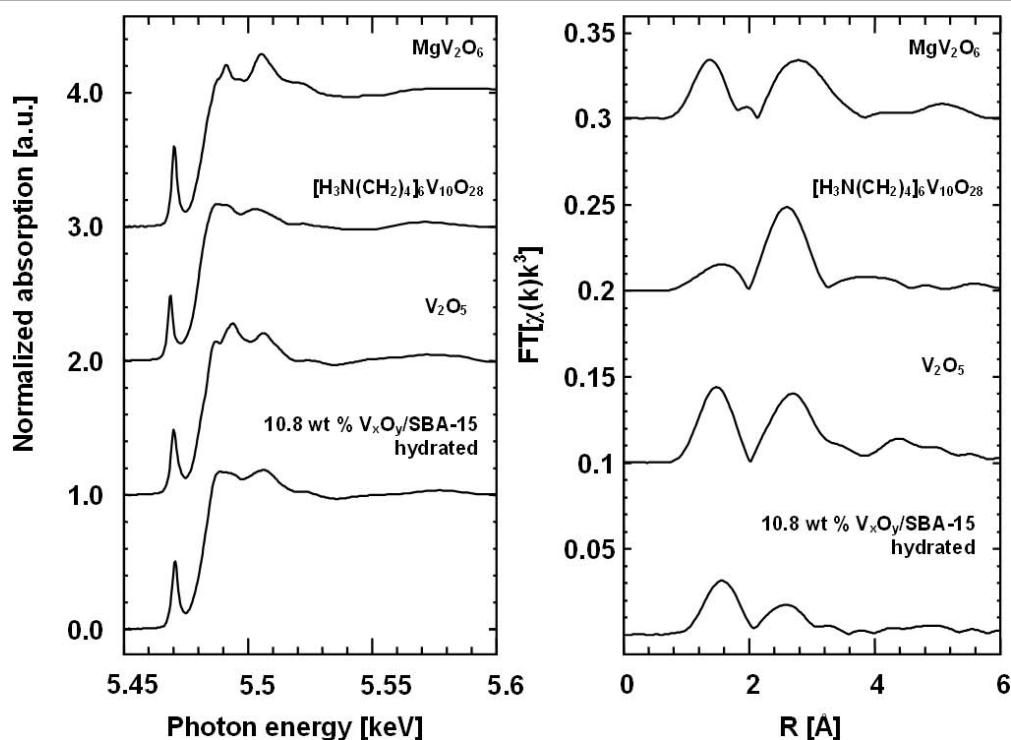
Figure 12 V K edge XANES spectra (a) and FT(χ(k)*k^3) of hydrated V$_x$O$_y$/SBA-15 (10.8 wt %) compared to those of various references (i.e. V$_2$O$_5$, [H$_3$N(CH$_2$)$_4$]$_6$V$_{10}$O$_{28}$, and MgV$_2$O$_6$).

FT(χ(k)*k^3) of hydrated V$_x$O$_y$/SBA-15 and V$_2$O$_5$ was obtained (Figure 13).

As described above, the validity of the XAFS analysis approach chosen was evaluated by calculating confidence limits and F parameters (Table 5). The model structure employed corresponds to the local structure around V centers in bulk V$_2$O$_5$ (Table 6). In fitting procedure #1 there V-O distances (1.6 Å, 1.8 Å, and 2.0 Å) and two σ^2 (one for R = 1.6 Å and one for all other

V-O distances) in the first V-O shell were allowed to vary independently. Additionally, three V-V distances (3.1 Å, 3.4 Å, and 3.6 Å) with the same σ^2 were refined. Moreover, E$_0$ was also allowed to vary in fitting procedure #1. Again because of N$_{ind}$ = 18 and N$_{free}$ = 10 refinement procedure #1 would be considered reliable according to the Nyquist criteria. Reasonable confidence limits and F = 0 were calculated for the V-V distances and σ^2(V-V) parameter. However, rather high

Table 5 Evaluation of EXAFS refinement of dehydrated V$_x$O$_y$/SBA-15.

		V$_2$O$_5$, procedure #1			V$_2$O$_5$, procedure #2			Hydrated V$_x$O$_y$-SBA-15		
Type	N	Z	± z	F	Z	± z	F	Z	± z	F
V - O	1	1.58	0.05	0.3	1.58	0.011	0	1.65	0.014	0
σ^2(V-O)	3(1)	0.011	0.0055	0.8	0.0104	0.0069	0	0.0126	0.0003	0
V - O	3(2)	1.87	0.06	0.3	1.88	0.014		1.92	0.018	0
σ^2(V-O)	-(3)	0.0098	0.004	0.8	-	-	-	-	-	-
V - O	-(1)	1.93	0.03	0.5	-	-	-	-	-	-
V - V	2	3.12	0.006	0	3.11	0.003	0	3.08	0.0075	0
σ^2(V-V)	3	0.0047	0.00032	0	0.0047	0.00035	0	0.013	0.0006	0
V - V	1	3.39	0.044	0	3.38	0.046	0	3.42	0.046	0.3
V - V	2	3.60	0.024	0	3.59	0.024	0	3.65	0.028	0
E$_0$	-	0.38	17.0	0.9	-	-	-	-	-	-

V K edge XAFS parameters (Z for distances R and disorder parameter σ^2) obtained from two different procedures of fitting a model structure (i.e. V$_2$O$_5$) to the experimental XAFS(FT(χ(k)*k^3)) of reference V$_2$O$_5$ and hydrated V$_x$O$_y$/SBA-15 (10.8 wt %) (details of fit given in Table 6) together with confidence limits (± z, referring to 95% of fit residual) and significance parameter F (details given in text). Fit residual 6.0 for V$_2$O$_5$ procedure #1, 6.3 for V$_2$O$_5$ procedure #2, and 13.6 for hydrated V$_x$O$_y$-SBA-15.
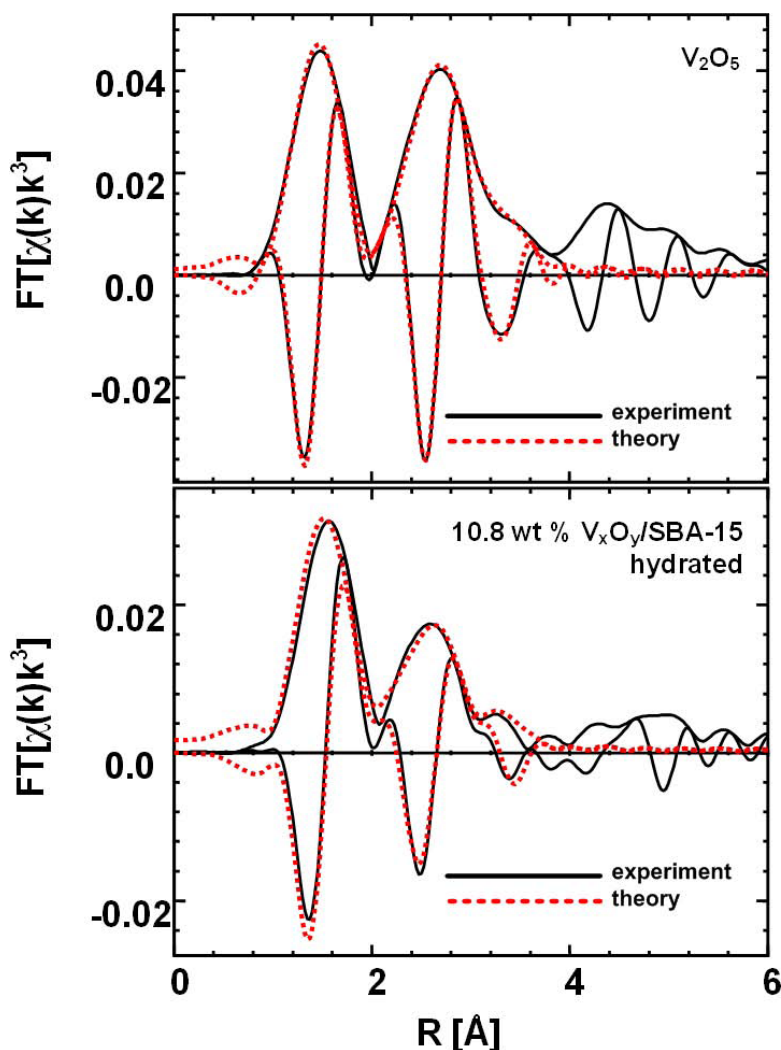
Figure 13 Experimental (solid) V K edge FT(χ(k)*k^3) of hydrated V_xO_y/SBA-15 (10.8 wt %) (bottom) and of V_2O_5(top) together with theoretical XAFS functions (V_2O_5 model).

confidence limits of the V-O distances of ± 0.05 Å and F parameters of 0.8 for both σ^2(V-O) parameters were obtained with procedure #1. Moreover, E_0 exhibited a confidence limit of ± 17.0 and F = 0.9. Hence, fitting procedure #1 clearly exceeds the number of meaningful parameters. Therefore, the fitting procedure was modified and the number of free parameters was reduced. E_0 was kept invariant again in the refinement, two V-O distances at ~1.6 Å and 1.9 Å, and one σ^2(V-O) parameter were used. In contrast to procedure #1, procedure #2 yielded reasonable confidence limits (e.g. ± 0.02 for V-O distances) and acceptable F parameters (mostly F = 0).

Table 5 indicates a small increase in the various V-O and V-V distances from V_2O_5 to hydrated V_xO_y/SBA-15. Intercalation of water in hydrated V_xO_y/SBA-15 may be accompanied by increasing nearest neighbor distances. More pronounced, though, is the increase in the

disorder parameter σ^2 for the V-O and V-V scattering scattering paths used in the XAFS refinement for hydrated V_xO_y/SBA-15 (Table 5). In particular, V-V contributions are strongly damped in the FT(χ (k)*k^3) of hydrated V_xO_y/SBA-15 indicating an increased disorder in the local structure of hydrated V_xO_y species supported on SBA-15 compared to bulk V_2O_5.

The structural similarity between hydrated vanadium oxide species supported on SiO_2 and V_2O_5 has previously been observed by Raman spectroscopy [10]. Evidently, the local structure of hydrated V_xO_y/SBA-15 used here is very similar to other materials previously described in the literature. Dehydration should therefore result in a similar structure of the dehydrated phase. In addition to 10.8 wt % V_xO_y/SBA-15, samples with lower loadings of 2.7 wt % and 5.4 wt % V were measured (Figure 10and Figure 11) and analyzed according to the

Table 6 EXAFS refinement results obtained for experimental FT(χ(k)*k^3) of hydrated V$_x$O$_y$/SBA-15 and V$_2$O$_5$.

Type	N	R_{Model} [Å]	V$_2$O$_5$ R [Å]	V$_2$O$_5$ σ^2 [Å^2]	hydrated V$_x$O$_y$-SBA-15 R [Å]	hydrated V$_x$O$_y$-SBA-15 σ^2 [Å^2]
V - O	1	1.58	1.58	0.0104	1.65	0.0126
V - O	1	1.78	1.88	0.0104$_C$	1.92	0.0126$_C$
V - O	2	1.88	1.88$_C$	0.0104$_C$	1.92$_C$	0.0126$_C$
V - O	1	2.02	1.88$_C$	0.0104$_C$	1.92$_C$	0.0126$_C$
V - V	2	3.08	3.11	0.0047	3.08	0.0129
V - V	1	3.43	3.39	0.0047$_C$	3.43	0.0129$_C$
V - V	2	3.56	3.59	0.0047$_C$	3.65	0.0129$_C$

Type and number (N) of atoms at distance R from the V atoms in a V$_2$O$_5$ system compared to experimental distances and XAFS disorder parameter (σ^2). Parameters were obtained from refinement of a V$_2$O$_5$ model structure (ICSD 60767) to the experimental V K edge XAFS FT(χ(k)*k^3) of hydrated V$_x$O$_y$/SBA-15 (10.8 wt %) and bulk V$_2$O$_5$(). (k range from 2.7 - 11.0 Å^{-1}, R range 0.9 - 3.8 Å, E$_0$ (V$_x$O$_y$/SBA-15) = 0.0 eV/E$_0$ (V$_2$O$_5$) = 0.0, fit residual 13.4 (V$_x$O$_y$/SBA-15) and 6.3 (V$_2$O$_5$), N$_{ind}$ = 18, N$_{free}$ = 7) (Subscript C indicates parameters that were correlated in the refinement). Confidence limits and significance of fitting parameters are given in Table 5.

procedure described above. Very similar results were obtained for the hydrated state of the low-loading samples compared to 10.8 wt % hydrated V$_x$O$_y$/SBA-15. Apparently, in the range of V loadings from ~3 to 11 wt % the local structure of both hydrated and dehydrated V$_x$O$_y$/SBA-15 is largely independent of the amount of vanadium oxide supported on SBA-15.

Conclusions

X-ray absorption spectroscopy is a very suitable technique for studying the local structure of dispersed metals or metal oxides on various support materials. Conventional XAFS analysis consists of finding a suitable model structure and fitting the corresponding theoretical XAFS functions to the experimental data. Because the number of potential parameters often exceeds the number of "independent" parameters, evaluating the reliability and significance of a particular fitting procedure is mandatory. Therefore, the number of independent parameters (Nyquist) alone is not sufficient. Here, we have employed confidence limits and F parameters to identify suitable analysis procedures. The local structure of vanadium oxide supported on nanostructured SiO$_2$ (SBA-15) was investigated. Three samples with different vanadium loadings (i.e. 2.7 wt %, 5.4 wt %, and 10.8 wt %) were employed. Thermal treatment in air at 623 K resulted in characteristic structural changes of the V oxide species. The local structure of dehydrated V$_x$O$_y$/SBA-15 was described best by assuming a model structure consisting of an ordered arrangement of neighboring V$_2$O$_7$ units. This is in good agreement with recent NEXAFS studies and theoretical calculations that also concluded the presence of V-V bonds in the V$_x$O$_y$ species supported on

SBA-15 [28]. Moreover, the local structures of both hydrated and dehydrated V$_x$O$_y$/SBA-15 were found to be independent of the V loading over the range employed. With respect to XAFS data previously presented in the literature and interpreted in terms of isolated VO$_4$ units it can be suggested that including contributions of higher shells would also lead to conclude polymeric V$_x$O$_y$ units. Comparing the influence of surface properties and structure of various support materials will be the subject of future work. Eventually, onset of catalytic activity in selective propene oxidation was detected at about 573 K. In situ XAS data measured under reaction conditions indicated, that the characteristic ordered arrangement of V$_2$O$_7$ dimers in the local structure of dehydrated V$_x$O$_y$/SBA-15 persisted. Future studies on V$_x$O$_y$ species supported on SBA-15 as model systems for vanadium based selective oxidation catalysts will have to take the presence of V$_2$O$_7$ species rather than isolated VO$_4$ units into account.

Experimental

Sample preparation

Silica SBA-15 was prepared according to literature procedures [2]. Details of preparation and characterization of the same catalysts were described elsewhere [9,10,14]. Briefly, SBA-15 was functionalized by adding 3-aminopropyltrimethoxysilane (APTMS) to a suspension of SBA-15 in toluene at 338 K. The suspension was stirred for 12 hours. The contents were filtered, washed and finally stirred in 0.3 M HCl for 12 hours. The contents was filtered again, washed with water and dried in air overnight (functionalized SBA-15). The vanadium oxides supported on SBA-15 were prepared by adding appropriate amounts of butylammonium decavanadate [31] to a suspension of functionalized SBA-15 in water. The resulting powder was calcined at 823 K for 12 hours. The results of the N$_2$ physisorption analysis of the SBA-15 and the SBA-15 supported vanadium oxide samples are given in and have been discussed in detail previously together with detailed structural characterization [10]. Importantly, in the presence of vanadium oxide the hexagonal structure of SBA-15 is preserved, the mesopores remain accessible to reactants, and the vanadia species are located inside the pores of SBA-15.

The vanadium oxides supported on SBA-15 obtained are denoted as hydrated V$_x$O$_y$/SBA-15 (as-prepared) or dehydrated V$_x$O$_y$/SBA-15 (after thermal treatment). In addition to V$_x$O$_y$/SBA-15 several vanadium oxide reference compounds with an average valance of +5 were measured. These were either used as-purchased (V$_2$O$_5$ (Alfa Aesar 99.8%), NH$_4$VO$_3$ (Riedel de Haën, 99.5%) and Na$_3$VO$_4$ (Alfa Aesar, 99.9%)) or were prepared according to literature procedures (Mg$_2$V$_2$O$_7$, MgV$_2$O$_6$, Mg$_3$V$_2$O$_8$ [32], and [H$_3$N(CH$_2$)$_4$]$_6$V$_{10}$O$_{28}$ [31]).

X-ray absorption spectroscopy (XAS)

In situ transmission XAS experiments were performed at the V K edge (5.465 keV) at beamline E4 at the Hamburg Synchrotron Radiation Laboratory, HASYLAB, using a Si(111) double crystal monochromator. The energy range used for V K near edge scans (XANES) and extended XAFS scans (EXAFS) was 5.4-5.7 keV (~3 min/scan) and 5.4-6.0 keV (~20 min/scan), respectively. For in situ and ex situ XAFS measurements samples were mixed with BN and PE, respectively, and pressed into self-supporting pellets (5 mm and 13 mm in diameter, respectively). In order to obtain an edge jump, $\Delta \mu_x$, at the V K below 1.0, 2 mg of 10.8 wt % and 5.4 wt % V_xO_y/SBA-15, 3 mg of 2.7 wt % V_xO_y/SBA-15, ~1 mg for bulk vanadium oxides (NH_4VO_3, V_2O_5, $[H_3N(CH_2)_4]_6V_{10}O_{28}$, Na_3VO_4) diluted with BN (~15 mg), and 3-6 mg for bulk vanadium oxides ($Mg_3V_2O_8$, MgV_2O_6) diluted with PE (~200 mg) were employed. Transmission XAS measurements were performed in an in situ cell described previously [33]. Dehydration of V_xO_y/SBA-15 was conducted in 20% O_2 and He (total flow 30 ml/min) in a temperature range from 293 K to 623 K at a heating rate of 5 K/min and a holding time of 30 min at 623 K. Reaction tests were performed in 5% propene and 6% O_2 in He in the temperature range from 293 K to 723 K (5 K/min, total flow 30 ml/min). The gas atmosphere was analyzed using a noncalibrated mass spectrometer in a multiple ion detection mode (QMS200 from Pfeiffer). Ex situ XAFS measurements were performed in He atmosphere at room temperature.

X-ray absorption fine structure (XAFS) analysis was performed using the software package WinXAS v3.2 [34]. Background subtraction and normalization were carried out by fitting linear polynomials to the pre-edge and 3rd degree polynomials to the post-edge region of an absorption spectrum, respectively. The extended X-ray absorption fine structure (EXAFS) $\chi(k)$ was extracted by using cubic splines to obtain a smooth atomic background $\mu_0(k)$. The FT($\chi(k)*k^3$), often referred to as pseudo radial distribution function, was calculated by Fourier transforming the k^3-weighted experimental $\chi(k)$ function, multiplied by a Bessel window, into the R space. EXAFS data analysis was performed using theoretical backscattering phases and amplitudes calculated with the ab-initio multiple-scattering code FEFF7 [35]. EXAFS refinements were performed in R space simultaneously to magnitude and imaginary part of a Fourier transformed k^3-weighted and k^1-weighted experimental $\chi(k)$ using the standard EXAFS formula [36]. This procedure strongly reduces the correlation between the various XAFS fitting parameters. Structural parameters allowed to vary in the refinement were (i) disorder parameter σ^2 of selected single-scattering paths assuming a symmetrical pair-distribution function and (ii) distances of selected single-scattering paths. Coordination numbers (CN), E_0 shifts, and amplitude reduction factor S_0^2 were kept invariant in the final fitting procedures. Correlations of specific parameters to reduce the number of free running parameters and to improve the stability of the refinement are described below.

The statistical significance of the fitting procedure employed was carefully evaluated in three steps. First, the number of independent parameters (N_{ind}) was calculated according to the Nyquist theorem $N_{ind} = 2/\pi*\Delta R*\Delta k + 2$. In all cases the number of free running parameters in the refinements was well below N_{ind}. Second, confidence limits were calculated for each individual parameter. In the corresponding procedure, one parameter was successively varied by a certain percentage (i. e. 0.05% for R and 5% for σ^2) and the refinement was restarted with this parameter kept invariant. The parameter was repeatedly increased or decreased until the fit residual exceed the original fit residual by more than 5%. Eventually, the confidence limit of the parameter was obtained from linear interpolation between the last and second last increment for an increase in fit residual of 5%. This procedure was consecutively performed for each fitting parameter. Third, a so-called F test was performed to assess the significance of the effect of additional fitting parameters on the fit residual. The corresponding procedure was adopted from the well-known library "Numerical Recipes in C" where it is described in detail [37]. In short, one parameter was varied by a certain percentage (i.e. between 2 and 8% for R and between 10 and 80% for σ^2) and the refinement was restarted with this parameter kept invariant. Subsequently, the difference between experimental and theoretical function (i.e. magnitude and imaginary part of FT ($\chi(k)*k^3$) for a refinement in R space) was calculated and compared to that of the original refinement. The corresponding F parameter ranges between 0.0 and 1.0, where F = 1.0 indicates an insignificant change in the fit residual, while F = 0.0 indicates a highly significant change in fit residual. The iterative procedure was terminated when the corresponding F parameter was below 0.7. Fit parameters with F = 0.8 or higher are most likely strongly correlated and may be statistically insignificant. These parameters should be kept invariant in the refinement. Eventually, this procedure was also consecutively performed for each fitting parameter.

Author details
[1]Institut für Chemie, Technische Universität Berlin, Strasse des 17. Juni 135, 10623 Berlin, Germany. [2]Fritz-Haber-Institute of the Max-Planck-Society, Department of Inorganic Chemistry, Faradayweg 4-6, 14195 Berlin, Germany. [3]Eduard-Zintl-Institut für Anorganische und Physikalische Chemie, Technische Universität Darmstadt, Petersenstr. 20, 64287 Darmstadt, Germany.

Authors' contributions
AW participated in XAFS data measurements and analysis, and drafted the manuscript. RH performed the sample preparation and N2 adsorption analysis. CH participated in design and coordination of the study, sample preparation, and N2 adsorption analysis. TR participated in XAFS data measurements and analysis, and design and coordination of the study. All authors read and approved the final manuscript.

Competing interests
The authors declare that they have no competing interests.

References
1. Ressler T, Walter A, Huang ZD, Bensch W: Structure and properties of a supported MoO_3-SBA-15 catalyst for selective oxidation of propene. *J Catal* 2008, **254**:170-179.
2. Zhao DY, Huo QS, Feng JL, Chmelka BF, Stucky GD: Nonionic Triblock and Star Diblock Copolymer and Oligomeric Surfactant Syntheses of Highly Ordered, Hydrothermally Stable, Mesoporous Silica Structures. *J Am Chem Soc* 1998, **120**:6024-6036.
3. Hess C: Characterization of the synthesis and reactivity behavior of nanostructured vanadia model catalysts using XPS and vibrational spectroscopy. *Surf Sci* 2006, **600**:3695-3701.
4. Hess C, Drake IJ, Hoefelmeyer JD, Tilley TD, Bell AT: Partial Oxidation of Methanol Over Highly Dispersed Vanadia Supported on Silica SBA-15. *Catal Lett* 2005, **105**:1-8.
5. Liu YM, Cao Y, Yi N, Feng WL, Dai WL, Yan SR, He HY, Fan KN: Vanadium oxide supported on mesoporous SBA-15 as highly selective catalysts in the oxidative dehydrogenation of propane. *J Catal* 2004, **224**:417-428.
6. Liu W, Lai SY, Dai H, Wang S, Sun H, Au CT: Oxidative dehydrogenation of n-butane over mesoporous VO_x/SBA-15 catalysts. *Catal Lett* 2007, **113**:147-154.
7. Keller DE, Visser T, Soulimani F, Koningsberger DC, Weckhuysen BM: Hydration effects on the molecular structure of silica-supported vanadiumoxide catalysts: A combined IR, Raman, UV-vis and EXAFS study. *Vib Spectrosc* 2007, **43**:140-151.
8. Venkov TV, Hess C, Jentoft FC: Redox Properties of Vanadium Ions in SBA-15-Supported Vanadium Oxide: An FTIR Spectroscopic Study. *Langmuir* 2007, **23**:1768-1777.
9. Hess C, Wild U, Schlögl R: The mechanism for the controlled synthesis of highly dispersed vanadia supported on silica SBA-15. *Microporous and Mesoporous Materials* 2006, **95**:339-349.
10. Hess C, Tzolova-Müller G, Herbert R: The Influence of Water on the Dispersion of Vanadia Supported on Silica SBA-15: A Combined XPS and Raman Study. *J Phys Chem C* 2007, **111**:9471-9479.
11. Hess C: Direct correlation of the dispersion and structure in vanadium oxide supported on silica SBA-15. *J Catal* 2007, **248**:120-123.
12. Oyama ST, Went GT, Lewis KB, Bell AT, Somorjai GA: Oxygen Chemisorption and Laser Raman Spectroscopy of Unsupported and Silica-Supported Vanadium Oxide Catalysts. *J Phys Chem B* 1989, **93**:6786-6790.
13. Gao X, Bare SR, Weckhuysen BM, Wachs IE: In Situ Spectroscopic Investigation of Molecular Structures of Highly Dispersed Vanadium Oxide on Silica under Various Conditions. *J Phys Chem B* 1998, **102**:10842-10852.
14. Hess C, Hoefelmeyer JD, Tilley TD: Spectroscopic Characterization of Highly Dispersed Vanadia Supported on SBA-15. *J Phys Chem B* 2004, **108**:9703-9709.
15. Schraml-Marth M, Wokaun A: Spectroscopic Investigation of the Structure of Silica-supported Vanadium Oxide Catalysts at Submonolayer Coverages. *J Chem Soc Faraday Trans* 1991, **87**(16):2635-2646.
16. Gao X, Wachs IE: Investigation of Surface Structures of Supported Vanadium Oxide Catalysts by UV-vis-NIR Diffuse Reflectance Spectroscopy. *J Phys Chem B* 2000, **104**:1261-1268.
17. Bronkema JL, Bell AT: Mechanistic Studies of Methanol Oxidation to Formaldehyde on Isolated Vanadate Sites Supported on MCM-48. *J Phys Chem C* 2007, **111**:420-430.
18. Olthof B, Khodakov A, Bell AT, Iglesia E: Effects of Support Composition and Pretreatment Conditions on the Structure of Vanadia Dispersed on SiO_2, Al_2O_3, TiO_2, ZrO_2, and HfO_2. *J Phys Chem B* 2000, **104**:1516-1528.
19. Keller DE, Koningsberger DC, Weckhuysen BM: Molecular Structure of a Supported VO_4 Cluster and Its Interfacial Geometry as a Function of the SiO_2, Nb_2O_5, and ZrO_2 Support. *J Phys Chem B* 2006, **110**:14313-14325.
20. Keller DE, Koningsberger DC, Weckhuysen BM: Elucidation of the molecular structure of hydrated vanadium oxide species by X-ray absorption spectroscopy: correlation between the V ... V coordination number and distance and the point of zero charge of the support oxide. *Phys Chem Chem Phys* 2006, **8**:4814-4824.
21. Keller DE, Airaksinen SMK, Krause AO, Koningsberger DC, Weckhuysen BM: Atomic XAFS as a Tool To Probe the Reactivity of Metal Oxide Catalysts: Quantifying Metal Oxide Support Effects. *J Am Chem Soc* 2007, **129**:3189-3197.
22. Keller DE, Weckhuysen BM, Koningsberger DC: Application of AXAFS Spectroscopy to Transition-Metal Oxides: Influence of the Nearest and Next Nearest Neighbour Shells in Vanadium Oxides. *Chem–Eur J* 2007, **13**:5845-5856.
23. Weckhuysen BM, Keller DE: Chemistry, spectroscopy and the role of supported vanadium oxides in heterogeneous catalysis. *Catal Today* 2003, **78**:25-46.
24. Tanaka T, Yamashita H, Tsuchitani R, Funabiki T, Yoshida S: X-Ray Absorption (EXAFS/XANES) Study of Supported Vanadium Oxide Catalysts. *J Chem Soc Faraday Trans* 1988, **84**(9):2987-2999.
25. Keller DE, de Groot FMF, Koningsberger DC, Weckhuysen BM: ËO$_4$ Upside Down: A New Molecular Structure for Supported VO_4 Catalysts. *J Phys Chem B* 2005, **109**:10223-10233.
26. Hawthorne FC, Calvo C: The crystal chemistry of the M^+VO_3 (M^+ = Li, Na, K, NH_4, Tl, Rb, and Cs) pyroxenes. *J Solid State Chem* 1977, **22**(2):157-170.
27. Gopal R, Calvo C: Crystal Structure of Magnesium Divanadate, $Mg_2V_2O_7$. *Acta Crystallogr, Sect B* 1974, **30**(10):B2491-2493.
28. Cavalleri M, Hermann K, Knop-Gericke A, Hävecker M, Herbert R, Hess C, Oestereich A, Döbler J, Schlögl R: Analysis of silica-supported vanadia by X-ray absorption spectroscopy: Combined theoretical and experimental studies. *J Catal* 2009, **262**:215-223.
29. Wong J, Lytle FW, Messmer RP, Maylotte DH: K-edge absorption spectra of selected vanadium compounds. *Phys Rev B* 1984, **30**:5596-5610.
30. Enjalbert R, Galy J: A Refinement of the Structure of V_2O_5. *Acta Crystallogr, Sect C* 1986, **C42**:1467-1469.
31. Roman P, Aranzabe A, Luque A, Gutierrez-Zorrilla JM: Preparation and solid state characterization of some alkylammonium decavanadates. Crystal structure of the hexakis(n-hexylammonium) decavanadate dihydrate. *Mater Res Bull* 1991, **26**:731-740.
32. Gao X, Ruiz P, Xin Q, Guo X, Delmon B: Preparation and characterization of three pure magnesium vanadate phases as catalysts for selective oxidation of propane to propene. *Catal Lett* 1994, **23**:321-337.
33. Ressler T, Jentoft RE, Wienold J, Günter MM, Timpe O: In Situ XAS and XRD Studies on the Formation of Mo Suboxides during Reduction of MoO_3. *J Phys Chem B* 2000, **104**:6360-6370.
34. Ressler T: WinXAS: a Program for X-ray Absorption Spectroscopy Data Analysis under MS-Windows. *J Synch Rad* 1998, **5**:118-122.
35. Rehr JJ, Booth CH, Bridges F, Zabinsky SI: X-ray-absorption fine structure in embedded atoms. *Phys Rev B* 1994, **49**:12347-12350.
36. Ressler T, Brock SL, Wong J, Suib SL: Multiple-Scattering EXAFS Analysis of Tetraalkylammonium Manganese Oxide Colloids. *J Phys Chem B* 1999, **103**:6407-6420.
37. Teukolsky A, Vetterling WT, Flannery BP: *Numerical Recipes: The Art of Scientific Computing* Cambridge: Cambridge University Press, Third 2007.